Journal of Colloid and Interface Science **243,** 248–254 (2001)
doi:10.1006/jcis.2001.7874, available online at http://www.idealibrary.com on IDEAL®

The Phase Behavior and Microstructure of Efficient Cationic–Nonionic Microemulsions

James A. Silas and Eric W. Kaler[1]

Center for Molecular and Engineering Thermodynamics, Department of Chemical Engineering, University of Delaware, Newark, Delaware 19716

Received May 30, 2001; accepted July 21, 2001; published online September 24, 2001

A surfactant mixture of didodecyldimethylammonium bromide (DDAB) and *n*-alkyl polyglycol ethers (C_iE_j) can make efficient microemulsions of decane and water. Increases in surfactant efficiency by up to a factor of four are realized as 2% C_8E_3 is replaced with DDAB. As little as 6% of an appropriate surfactant mixture can microemulsify equal masses of oil and water. The increase in DDAB concentration causes the spacing of the bicontinuous domains of oil and water to decrease and the correlation length of the surfactant monolayers to increase. These changes in structural parameters, as detected by small-angle neutron scattering, are in quantitative accord with theoretical calculations of changes in structure as a result of electrostatic stiffening of elastic membranes. Although the reported changes in microstructure are consistent with predictions, they alone cannot explain the observed large increases in overall surfactant efficiency.

Key Words: **microemulsion; surfactant mixture; phase behavior; SANS; microstructure; bending modulus.**

INTRODUCTION

Microemulsions are thermodynamically stable, isotropic, microstructured solutions of surfactant, oil, and water. Their microstructure depends on the organization of a surfactant rich film that separates oil and water domains which have characteristic dimensions of 10–500 nm. The thermodynamic, structural, and dynamic properties of microemulsions have received much attention in recent years (1, 2). For economic reasons, the search is still active for conditions that allow solubilization of oil and water using the least amount of surfactant. Many strategies have been employed to increase the efficiency of surfactants, such as by blending nonionic surfactants with block copolymers (3) or ionic cosurfactants (4–7).

Adding an anionic cosurfactant increases the surfactant efficiency of *n*-alkyl polyglycol ethers (C_iE_j's) with alkane oils (6) and glucoside surfactants with ether oils (7). The addition of less than 5% anionic to nonionic surfactant can reduce the amount of surfactant needed to solubilize equal amounts of oil and water by a factor of four. Phenomenologically, these observations are rationalized in terms of the hydrophilic–lipophilic balance (HLB) of the surfactant mixture (4, 8, 9), or the relative location of the surfactant—water critical point (10–14). Many of the structural aspects of anionic–nonionic surfactant mixtures have been observed in droplet and lamellar phases, including changes in phase progression (15, 16), droplet size, and lamellar spacing (17, 18).

Studies of the effect of a cationic surfactant on microemulsions formed with ethoxylated alcohol surfactant are less common, but results reported recently do not differ greatly from those for anionic–nonionic surfactant mixtures. For didodecyldimethylammonium bromide (DDAB) with $C_{12}E_5$, small-angle neutron scattering (SANS), combined with pulsed field gradient NMR, indicates that DDAB remains mainly at the internal interface and does not partition appreciably into either the oil or water domains (19). This implies that the cationic surfactant directly alters the composition of the surfactant film, and leads to phase behavior similar to that of anionic–nonionic surfactant mixtures (15, 20).

Theory suggests that the microstructure and phase behavior of microemulsions depend on the properties of the surfactant rich film that separates oil and water domains (21, 22). This film is characterized by its spontaneous curvature (c_0), Gaussian bending modulus (k), and saddle-splay modulus (k), which depend on the molecular details of the interactions of oil, water, and surfactant. Safran and co-workers have described the surfactant-rich film in terms of these three parameters and have reproduced many aspects of surfactant solutions (21, 23, 24). The contribution of the electric double layer to the Gaussian bending modulus of a charged surfactant film can be calculated, and this result combined with the Safran approach can predict the effect of ionic surfactant on the microstructure of a nonionic surfactant film.

The use of this approach to analyze the addition of ionic surfactant to nonionic bilayers in a lamellar phase shows that the bending modulus of the nonionic bilayer increases with the addition of ionic surfactant (17). This increase is due to the formation of an electrical double layer on either side of the bilayer. The change in bending modulus causes a measurable change in the distance between successive bilayers that is consistent with theoretical calculations.

The interdomain spacing and surfactant persistence lengths of a bicontinuous microemulsion can be obtained from SANS spectra using a model developed by Teubner and Strey (25). The

[1] To whom correspondence should be addressed. Fax: 302-831-6751. E-mail: kaler@che.udel.edu.

0021-9797/01 $35.00

addition of an ionic cosurfactant alters the spacing and persistence length of the microstructure in ways that are detectable with SANS, and these parameters yield information about the properties of the surfactant film. By holding the total surfactant concentration constant, the effect of increasing the ionic surfactant concentration can be determined independently from the effect of total surfactant concentration.

MATERIALS AND METHODS

Materials

n-Octyl trioxyethylene glycol ether (>99%), C_8E_3, and *n*-dodecyl trioxyethylene glycol ether (>99%), $C_{12}E_3$, were obtained from Nikko. Water was filtered through a 0.2-μm filter, distilled, and deionized until the specific resistance was 18.3 MΩ cm. Decane (>98%) was purchased from Fluka. DDAB (>99%) was obtained from TCI America. D_2O (99.9%, DLM-11) was obtained from Cambridge Isotopes. All materials were used without further purification.

Phase Behavior Determination

The procedure used for ternary and quaternary phase diagram determination follows the method introduced by Kahlweit and co-workers (26, 27). A four-component phase space is defined by temperature, pressure, and three composition variables. The following composition variables are used to specify the amount of (A) water, (B) oil, (C) nonionic surfactant, and (D) ionic surfactant: The mass fraction of oil neglecting surfactant, α, is defined as

$$\alpha = \frac{\mathrm{B}}{\mathrm{A}+\mathrm{B}} \times 100, \qquad [1]$$

the mass fraction of surfactant, γ, is defined as

$$\gamma = \frac{\mathrm{C}+\mathrm{D}}{\mathrm{A}+\mathrm{B}+\mathrm{C}+\mathrm{D}} \times 100, \qquad [2]$$

and the mass fraction of ionic surfactant in the surfactant mixture, δ, is defined as

$$\delta = \frac{\mathrm{D}}{\mathrm{C}+\mathrm{D}} \times 100. \qquad [3]$$

For a ternary mixture, $\delta = 0$. If salt is added to the solution, the weight concentration of salt in water is defined as ε, and the weight of the brine is used in the above equations as A. To represent the phase space in two dimensions, only two of the defining variables can vary. At constant pressure, the phase behavior can be read as a function of temperature against one composition variable, with all others being held constant.

Sections through the phase prism at $\alpha = 50$ are used to determine the least amount of surfactant needed to solubilize equal weights of oil and water. This occurs at $\gamma = \tilde{\gamma}$ and $T = \tilde{T}$, where the one- and three-phase regions meet at a point at $\alpha = 50$. The surfactant concentration, $\tilde{\gamma}$, is called the efficiency of the surfactant. Varying the surfactant composition allows tracking of surfactant efficiency as a function of δ.

Neutron Scattering

Neutrons of $\lambda = 6$ Å with $\Delta\lambda/\lambda = 10\%$ were collimated and focused on thermally equilibrated samples held in quartz banjo cells in a 30 m spectrometer at the National Institute of Standards and Technology Cold Neutron Research Facility (NIST-CNRF) in Gaithersburg, MD. Detector distances of 1, 4.5, and 13 m were used to obtain spectra over q-values from 0.004 to 0.5 Å^{-1}. The detector was offset 25 cm for detector distances of 1 and 4.5 m to provide adequate overlap for combining data sets. Scattering spectra were corrected for background, empty cell scattering, and detector sensitivity and were placed on absolute scale through the use of water and silica standards provided by NIST.

Neutron Scattering Theory—Teubner–Strey Scattering

Teubner and Strey developed a phenomenological model to describe scattering from bicontinuous microemulsions (25). The model captures the major features of many experimental spectra and gives information about the structure and interactions within the solution. In this model the scattered intensity is given by

$$I_{\mathrm{TS}}(q) = \frac{8\pi c_2 \langle \eta^2 \rangle / \xi}{a_2 + c_1 q^2 + c_2 q^4}, \qquad [4]$$

where $\langle \eta^2 \rangle \equiv \phi_a(1-\phi_a)\langle \Delta\rho^2 \rangle$, and $\langle \Delta\rho^2 \rangle$ is the difference in scattering length density between media a and b. The term ϕ_a is the volume fraction of media a while $(1-\phi_a)$ is the volume fraction of media b. This corresponds to an isotropic real space correlation function, $\gamma(r)$, that incorporates alternating regions of water and oil,

$$\gamma(r) = \frac{\sin(kr)}{kr} \exp\left(-\frac{r}{\xi}\right), \qquad [5]$$

where $k = 2\pi/d$. The two length scales in the solution, d and ξ, are related to a_1, c_1, and c_2 via

$$\frac{d}{2\pi} = \left[\frac{1}{2}\left(\frac{a_2}{c_2}\right)^{1/2} - \frac{c_1}{4c_2}\right]^{-1/2} \qquad [6]$$

$$\xi = \left[\frac{1}{2}\left(\frac{a_2}{c_2}\right)^{1/2} + \frac{c_1}{4c_2}\right]^{-1/2}. \qquad [7]$$

The length scale d represents a quasi-periodic repeat distance between polar and nonpolar regions within the solution, while the correlation length ξ corresponds to a characteristic length for positional correlation.

Microemulsion structure ranges from a completely disordered solution to the ordering more characteristic of a lamellar phase.

An amphiphilicity factor, f_a, can be defined in terms of the coefficients a_2, c_1, c_2 as (28, 29)

$$f_a = \frac{c_1}{(4a_2c_2)^{1/2}}. \quad [8]$$

The value of f_a ranges from 1 for a completely disordered solution to -1 for a lamellar phase. The Lifschitz line is crossed when $f_a = 0$, and at this point a peak in the scattering spectra is observed at nonzero wave vector. The amphiphilicity factor provides a very useful absolute scale for the quantification of ordering in microemulsions.

PHASE BEHAVIOR

Results

C_iE_j/DDAB/water. The addition of small amounts of DDAB greatly influences the aqueous phase behavior of both $C_{12}E_6$ and C_8E_3 (Fig. 1). The lower consolute point that characterizes the usual phase behavior of ethoxylated alcohol surfactants moves to higher temperatures upon the addition of DDAB, while at the same time, a lamellar phase begins to form at high temperatures with only small concentrations of cosurfactant. Thus, DDAB increases the micellar region on the surfactant–water pseudo-binary and stabilizes a lyotropic phase at small overall surfactant concentrations. The lower temperature boundary of the multiphase lamellar region shown in Fig. 1 is constant upon further addition of DDAB (higher δ's), so that the largest phase behavior changes occur with the initial additions.

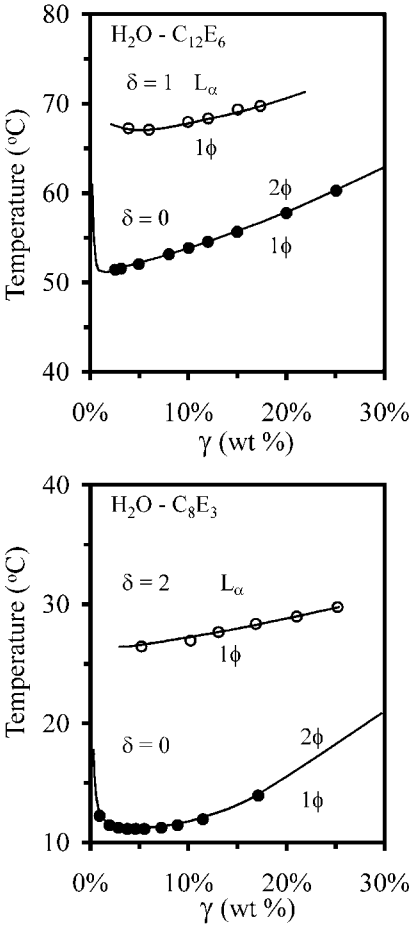

FIG. 1. Pseudo-binary surfactant water phase diagrams of $C_{12}E_6$ and C_8E_3 with added DDAB. The phase L_α represent both single and multiphase lamellar regions. The lamellar phase boundary does not change upon further addition of DDAB.

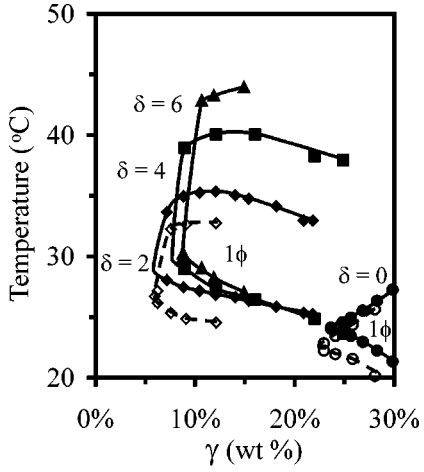

FIG. 2. Pseudo-ternary cut through the phase prism at $\alpha = 50$ and various δ. The closed symbols represent the phase behavior in water while the open symbols represent the phase behavior in D_2O. Only the single-phase microemulsions are shown for clarity.

C_8E_3/DDAB/decane/water. The efficiency of C_8E_3 with decane greatly increases with the addition of DDAB (Fig. 2). At $\delta = 2$, the value of $\tilde{\gamma} = 6$ represents an increase in the efficiency of the surfactant mixture by a factor of 4, from $\tilde{\gamma} = 23$ at $\delta = 0$. Further addition of DDAB decreases the overall efficiency of the surfactant mixture, while increasing the temperature stability of the one-phase microemulsion. At $\delta = 2$, the temperature range of the one-phase microemulsion is 8°C, while at $\delta = 6$, the temperature range of the one-phase microemulsion is 17°C. Most of the increase in microemulsion stability results from the upper phase boundary moving to higher temperatures with the addition of DDAB, as the lower phase boundary of the one-phase region remains relatively constant. Substituting D_2O for H_2O shifts the phase boundaries down by a few degrees Celsius (see Fig. 2).

Discussion

Changes in the phase behavior of C_iE_j–water upon the addition of DDAB have been reported previously in conjunction with a study of silicone oils (20). In general, the addition of an ionic surfactant to ethoxylated alcohols decreases their hydrophobicity. This increases the critical point on the surfactant–water binary, T_β, and as reported for the silicone oils, increases T_α, the upper consolute temperature on the surfactant–oil binary. Combined, these effects contribute to the observed increase in the

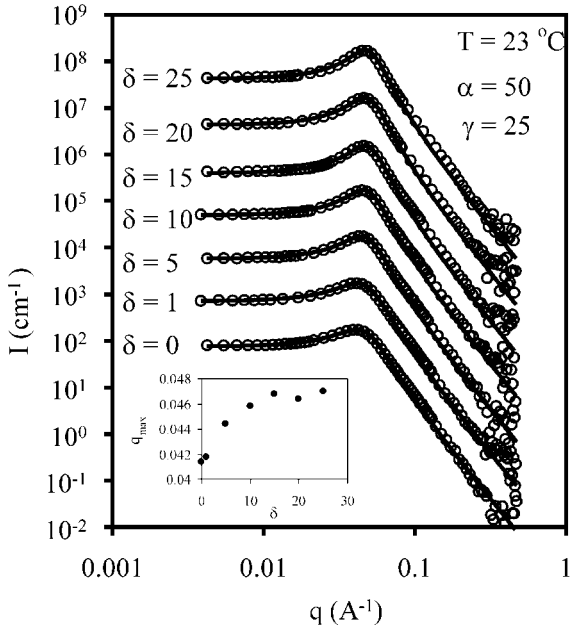

FIG. 3. SANS spectra for C_8E_3–DDAB–Decane–D_2O solutions at $\gamma = 25$, $\alpha = 50$, and $T = 23°C$. The spectra for $\delta = 0$ is on absolute scale, with each successive spectra offset by a factor of 10. Solid lines are fits to the model of Teubner and Strey (25). Inset indicates the q-position of the peak maximum (q_{max}) as a function of δ on a linear scale to illustrate the peak shift.

temperature of the single-phase microemulsion shown in Fig. 2, as the surfactant requires higher temperatures to partition into the oil phase. Further increases in ionic surfactant concentration serve to make the microemulsions less temperature sensitive, as the upper phase boundary on the single-phase microemulsion increases in temperature with δ, while the lower phase boundary remains relatively constant. The addition of an ionic surfactant to make a temperature insensitive microemulsion has been reported previously (30–32), and reflects the fact that DDAB partitions into the surfactant film.

Interestingly, the increase in efficiency between C_8E_3 and C_8E_3 with DDAB is about a factor of 4 for both decane and the silicone oil octamethylcyclotetrasiloxane, (D_4). However, for the silicone oil, $\delta = 18$ is needed to obtain the most efficient microemulsions, while $\delta = 2$ is sufficient for decane. Whether this is due to the difference in molecular weight (about a factor of 2) or to more specific chemical factors remains an open question.

In order to examine changes in microstructure, it is useful to note that all the mixtures shown in Fig. 2 with DDAB share the single-phase region of the original nonionic microemulsion at $\gamma = 25$ and $T = 23°C$. This allows measurement of changes in microstructure that occur as δ varies while keeping all other composition variables and temperature constant. Measurement of the microstructure in the efficient microemulsions, as δ increases, would also be useful in determining the effect of ionic surfactant. Because these microemulsions are highly efficient, they have a microstructure that is relatively large, so the samples scatter neutrons strongly and multiple scattering can distort and obscure otherwise useful data (33).

NEUTRON SCATTERING

Results for $\gamma = 25$ Microemulsions

Small but systematic changes in scattering spectra as a function of δ are shown in Fig. 3. All the solutions were equilibrated as a single phase at $\alpha = 50$, $\gamma = 25$, $T = 23°C$, and various δ, with the subsequent spectra offset by factors of 10 for clarity. The overall form of $I(q)$ remains constant, while the position and shape of the main peak systematically changes as δ increases. The inset shows the movement in peak position on a linear scale for the solutions in Fig. 3. The solid lines correspond to fits of the data to Eq. [4] for scattered intensity derived by Teubner and Strey (25). From each fitted curve, the domain spacing d, correlation length ξ, and amphiphilicity factor f_a, are obtained (Fig. 4 and Table 1). Since only δ varies, the shifts in d, ξ, and

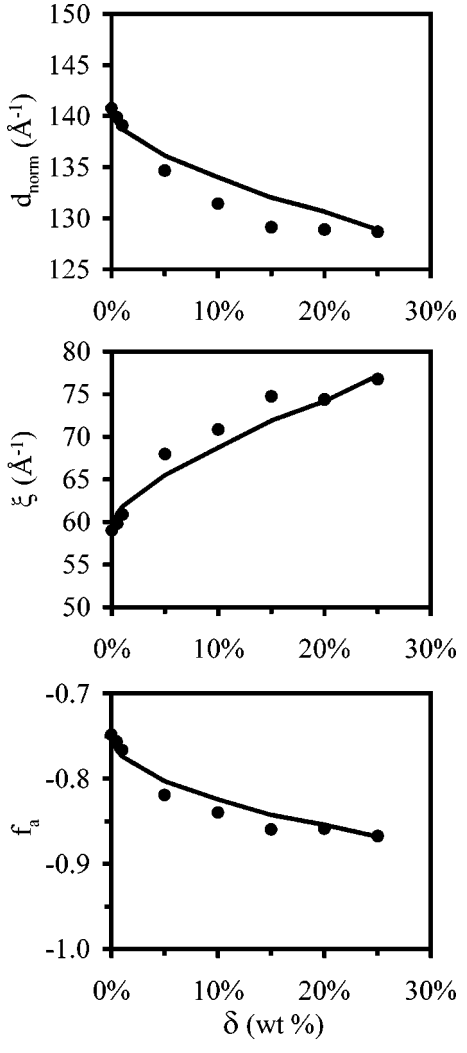

FIG. 4. Parameters from Teubner–Strey (25) fits are shown with closed symbols. d_{norm} is corrected for experimental variations in total surfactant concentration. Solid lines represent the theoretical scaling derived in Eqs. [14], [11], and [15].

TABLE 1
Sample Compositions and Tuebner–Strey (25) Fitted Parameters for C_8E_3–DDAB–Decane–D_2O SANS Spectra in Fig. 3

γ	α	δ	D (Å)	D_{norm} (Å)	ξ (Å)	f_a
25.0	49.9	0	140.8	140.8	58.6	−0.746
25.0	50.0	0.5	139.8	139.9	59.8	−0.757
24.8	50.0	1	140.2	139.1	60.3	−0.760
25.1	50.3	5	134.5	134.7	67.6	−0.818
25.1	50.2	10	131.1	131.4	71.0	−0.841
25.0	49.4	15	129.1	129.1	75.0	−0.860
25.0	50.5	20	129.1	128.9	76.7	−0.863
25.0	49.9	25	128.8	128.7	77.1	−0.868

Note. γ, α, and δ are the sample compositions in weight percent. The domain spacing D is normalized by the surfactant volume fraction to yield D_{norm}.

f_a are attributed to the charging of the nonionic microemulsion with the cationic DDAB.

To account for small variations in the experimental values of γ, the overall surfactant volume fraction was normalized to the original microemulsion surfactant volume fraction (34, 35). Therefore, the normalized repeat spacing corresponds to $d\phi/\phi_0$. The resulting corrections are less than 1% of the experimental values and are displayed as d_{norm} in Table 1 and Fig. 4.

Discussion

As δ increases, the repeat spacing d decreases and the correlation length ξ increases. Thus, the surfactant layers are slightly closer together and correlated over longer length scales as δ increases. This increase in order can be quantified by the value of the amphiphilicity factor f_a, which decreases from -0.75 to -0.85 as δ increases from 0 to 25. Adding DDAB (increasing δ) therefore moves the solution structure toward a more lamellar-like ordering as δ increases.

If the surfactant monolayer is modeled as an elastic membrane, the evolution of microstructure can be related to the membraane properties. The contribution of the electric double layer to the bending modulus of surfactant monolayers is (22)

$$\frac{k_{el}}{k_B T} = \frac{3\pi \ell |\sigma|^2}{2\kappa^3 e^2}, \qquad [9]$$

where k_B is Boltzmann's constant, T is temperature, ℓ is the Bjerrum length, σ is the surface charge density, κ is the inverse Debye length, and e is the charge of an electron. Under the assumptions that all the ionic surfactant is co-assembled with the nonionic surfactant (19), that all the counter-ions are disassociated and in a dielectric medium with properties that are the volumetric average of those of water and ethylene oxide head groups, and that the nonionic surfactant does not change its conformation at the interface in the presence of ionic surfactant, the electrostatic contribution to the bending modulus can be calculated as a function of the composition of the solutions (Fig. 5). Given that the bare bending modulus for C_8E_3 with decane is about 0.5 k_BT (35), the calculated increase in k resulting from the formation of an electrostatic double layer is about 10%.

This increase in k drives microstructure changes because the persistence length of an elastic membrane is related to k via (23)

$$\xi_k = a \exp\left[\frac{4\pi k}{3k_B T}\right], \qquad [10]$$

where a is a length of molecular size and $k = k_0 + k_{el}$. While in some cases the persistence length measured by SANS, ξ, has been set equal to the persistence length of the elastic membrane, ξ_k (35), this may not be generally true. Nonetheless, ξ and ξ_k should scale similarly, and so

$$\frac{\xi}{\xi_0} = \exp\left[\frac{4\pi k_{el}}{3k_B T}\right], \qquad [11]$$

where ξ_0 is $\xi(\delta = 0)$. Thus, the progression of ξ with δ can be predicted using only the values given in Fig. 5, and this is shown in Fig. 4. The good agreement between experiment and theory indicates that the change in correlation length can be accounted for by only the additional contribution to the bending modulus as a result of the deformation of the electric double layer.

To calculate the change in repeat spacing as ionic surfactant is added to the system, consider the surfactant monolayers to pack in a planar array, and so $d \sim 1/\phi_s$ (34, 35). Similarly, d should scale with the effective, or projected, surfactant area, $d \sim 1/A_{projected}$. Given an expression for the extensional modulus of fluctuating membranes, the excess area (that area consumed by out-of-plane fluctuations, A_{XS}) over the projected area is (23)

$$\frac{A_{XS}}{A_{projected}} = \frac{k_B T}{4\pi k} \ln\left(\frac{L}{a}\right), \qquad [12]$$

where L, and a are length scales that correspond to the upper and lower cutoffs of the experimental technique. Since the surfactant,

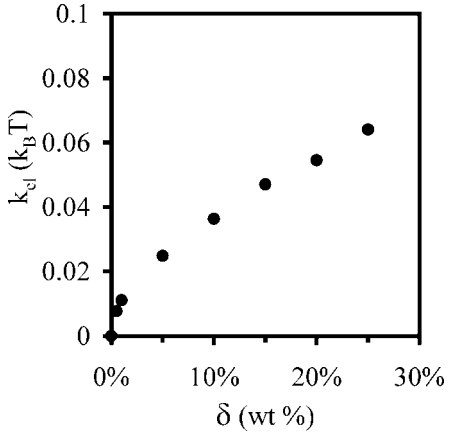

FIG. 5. The calculated electrostatic contribution to the bending modulus. The bare nonionic value for C_8E_3 with decane is about 0.5 kT (35).

water, and oil concentrations remain constant as δ increases, two conservation equations hold. Applying conservation of total surfactant area, $A_{\text{total}} = A_{\text{projected}} + A_{\text{XS}}$, and total volume of the solubilized phases yields

$$\frac{d}{d_0} = \frac{1 + \frac{\beta}{k}}{1 + \frac{\beta}{k_0}}, \qquad [13]$$

where d is the repeat spacing of the surfactant layers, d_0 is the repeat spacing of the nonionic system ($\delta = 0$), β is a constant of order $k_B T$, k_0 is the bending modulus of the bare nonionic monolayer, and $k = k_0 + k_{\text{el}}$. Since k_{el} is small compared to k_0,

$$\frac{d}{d_0} \approx 1 - k_{\text{el}}\left(\frac{\beta}{k_0^2 + \beta k_0}\right). \qquad [14]$$

Taking $\beta = k_B T$, $k_0 = 0.5\, k_B T$, and k_{el} as the calculated values in Fig. 5, the scaling of d is plotted in Fig. 4 and compared to the normalized domain spacing d_{norm}. The agreement between the theoretical scaling and experimental values indicates that the decrease in domain spacing is consistent with the calculated increase in the bending modulus as a result of electrostatics.

Once the domain spacing and persistence length are determined, the amphiphilicity factor scaling follows directly since (28, 29)

$$f_a = \frac{\left(\frac{d}{2\pi\xi}\right)^2 - 1}{\left(\frac{d}{2\pi\xi}\right)^2 + 1}. \qquad [15]$$

Since d decreases and ξ increases with increasing k_{el}, the calculated amphiphilicity factor decreases from its nonionic value as δ increases (Fig. 4).

Overall, there is good agreement between the microstructural parameters measured using SANS and theoretical scaling based upon how the calculated charge of the surfactant film modifies its bending modulus. Physically, as the bending modulus increases, the amount of excess area decreases. Because of conservation of surfactant area, the projected area of the surfactant film increases. However, since the increase in projected area cannot be accompanied by an increase in solubilized volume, the domain spacing must decrease to accommodate the larger projected area of the surfactant film. These results all conform to the picture of ionic surfactant co-assembling with nonionic surfactant, increasing the bending modulus through electrostatic charge, suppressing undulations of the nonionic surfactant film, and recovering lost surfactant area by increasing the ordering of the surfactant film. Nonetheless, the calculated and experimentally measured values for the change in bending modulus consistently account for an increase in surfactant area of about 10%. This is far less than that required to stabilize a bicontinuous microemulsion with increases in surfactant efficiencies of 400%, as shown in Fig. 2.

In order to understand the increase in surfactant efficiency, it is helpful to consider the various phase boundaries. As surfactant concentration decreases, the single-phase microemulsion will, depending on the temperature, separate to form an excess oil phase, an excess water phase, or both. The shape of the one-phase region (the so-called fish tail) corresponds to two separate emulsification failures with respect to either water or oil. With increasing δ, the boundary at lower temperature remains constant, both here and in other experimental systems (6, 7). This boundary corresponds to the emulsification failure of oil, i.e., where the single-phase microemulsion does not swell further with oil. The addition of DDAB does not affect this phase boundary.

The upper phase boundary, however, increases with each successive addition of ionic surfactant. This boundary corresponds to the emulsification failure of water, i.e., where the single-phase microemulsion does not swell further with water. The large change in the phase boundary for the formation of an aqueous excess phase compared to the negligible change for formation of an oily excess phase suggests an important role for the soluble counter-ions and the significance of the relative dilution of ions between the excess and microemulsion phases. Since electrostatic neutrality within any phase implies the counterions accompany the ionic surfactant, osmotic effects should cause the microemulsion to swell with water and therefore delay the formation of the mostly water excess phase with an increase in temperature. The asymmetry between the lower and upper phase boundary is consistent with a substantial role for osmotic effects, since the counterions are only soluble in the water domains.

Figure 6 shows the effect of increasing salt concentration (NaBr) on the phase behavior of C_8E_3–DDAB surfactant mixtures. The addition of salts to nonionic surfactant solutions shifts

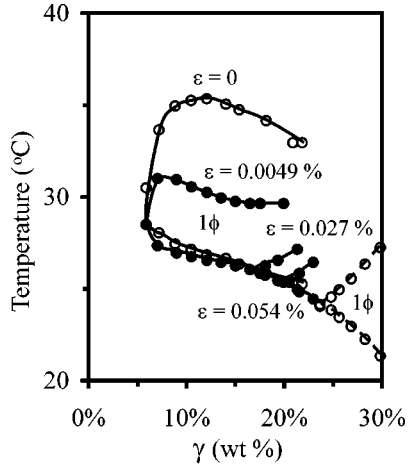

FIG. 6. The effect of added NaBr on the phase behavior of C_8E_3–DDAB–decane–H_2O at $\alpha = 50$ and $\delta = 2$ are shown with closed symbols. ε's represent weight percent of NaBr in water. Open symbols are the same system for $\varepsilon = 0$. Only one-phase microemulsions are shown for clarity.

the temperature of the surfactant–water miscibility gap by a few degrees celsius per wt% salt in water. The addition of NaBr will also modify any osmotic driving force present in the chemical potential of the ionic surfactant or counterions. The smallest addition of salt ($\varepsilon = 0.0049\%$) reduces the temperature stability of the single-phase microemulsion, while the surfactant mixture remains just as efficient. The concentration of added ions (0.001 M) is about 1/6 the concentration of counterions from DDAB at $\tilde{\gamma} = 7\%$. As the amount of added NaBr increases to $\varepsilon = 0.027$ and 0.054%, the efficiency of the surfactant mixture decreases to the bare nonionic surfactant efficiency in much the same way that it increased upon the addition of DDAB. The lower phase boundary remains stationary in temperature while the upper phase boundary decreases in temperature. At the $\tilde{\gamma}$ of the two higher salt concentrations ($\varepsilon = 0.0027$ and 0.0054%), the concentration of added salt ions (0.05 M and 0.008 M) is one-half the concentration of counterions from DDAB. Calculations of the electrostatic contribution to the bending modulus indicate that solutions at $\varepsilon = 0.0054\%$ still have half the magnitude of $\varepsilon = 0$ solutions, while the efficiency is nearly that of the nonionic microemulsion. The effect of salt concentrations this low on the phase behavior of the nonionic surfactant is negligible, and so the main effect is the modification of the electrostatics in solution. Given that this four-component mixture is a one-phase solution, and that the ionic surfactant is practically insoluble in either excess phase, appropriate theory should be able to evaluate the relative stability of the microemulsion phase versus an excess water phase.

Finally, it is interesting to note that while the change in microstructure in the bicontinuous phase as ionic surfactant is added is fully explained by the theoretically calculated changes in bending modulus, the enhanced stability of the single-phase microemulsion depends on the detailed thermodynamics of both the microemulsion and the excess phases.

SUMMARY

The addition of cationic surfactant increases the efficiency of ethoxylated alcohol surfactants to form microemulsions with decane. These results are similar to those for anionic C_iE_j–surfactant mixtures. SANS measurements of a single composition of surfactant, oil, and water as a function of the composition of the surfactant mixture shows the changes in bicontinuous microstructure as a function of added charge. These results correspond to the changes predicted as the consequence of a change in bending modulus as ionic surfactant is added. The bending modulus increases by about 10% as δ increases to 25, with the resulting changes in repeat length and correlation length indicating an increase in correlated structure in the microemulsion. The coincidental increase in surfactant efficiency is not completely explainable in these terms but is likely related to the change in the thermodynamics of emulsification failure toward water as the counterions of the surfactant modify the chemical potential of water.

ACKNOWLEDGMENTS

The authors acknowledge useful discussions with Randal Hill. This work was supported by Dow Corning.

REFERENCES

1. Strey, R., *Curr. Opin. Colloid Interface Sci.* **1,** 402 (1996).
2. Schubert, K.-V., and Kaler, E. W., *Ber. Bunsenges. Phys. Chem.* **100,** 190 (1996).
3. Jakobs, B., Sottman, T., Strey, R., Allgaier, J., Willner, L., and Richter, D., *Langmuir* **15,** 6707 (1999).
4. Kunieda, H., Hanno, K., Yamaguchi, S., and Shinoda, K., *J. Colloid Interface Sci.* **107,** 129 (1985).
5. Kahlweit, M., and Strey, R., *J. Phys. Chem.* **92,** 1557 (1988).
6. Kahlweit, M., Faulhaber, B., and Busse, G., *Langmuir* **10,** 2528 (1994).
7. Ryan, L. D., and Kaler, E. W., *J. Phys. Chem.* **102,** 7549 (1998).
8. Aramaki, K., Ozawa, K., and Kunieda, H., *J. Colloid Interface Sci.* **196,** 74 (1997).
9. Shinoda, K., Kunieda, H., Arai, T., and Saijo, H., *J. Phys. Chem.* **88,** 5126 (1984).
10. Marszall, L., *Langmuir* **6,** 347 (1990).
11. Marszall, L., *Langmuir* **4,** 90 (1988).
12. Douglas, C. B., and Kaler, E. W., *J. Chem. Soc., Faraday Trans.* **90,** 471 (1994).
13. Douglas, C. B., and Kaler, E. W., *Langmuir* **10,** 1075 (1994).
14. Firman, P., Haase, D., Jen, J., Kahlweit, M., and Strey, R., *Langmuir* **1,** 718 (1985).
15. Rajagopalan, V., Bagger-Jörgensen, H., Fukuda, K., Olsson, U., and Jönsson, B., *Langmuir* **12,** 2939 (1996).
16. Douglas, C. B., and Kaler, E. W., *Langmuir* **7,** 1097 (1991).
17. Schomäcker, R., and Strey, R., *J. Phys. Chem.* **98,** 3908 (1994).
18. Fukuda, K., and Olsson, U., *Langmuir* **10,** 3222 (1994).
19. Giustini, M., Palazzo, G., Ceglie, A., Eastoe, J., Bumujad, A., and Heenan, R. K., *Progr. Colloid Polym. Sci.* **115,** 25 (2000).
20. Silas, J. A., Kaler, E. W., and Hill, R. M., *Langmuir* **17,** 4534 (2001).
21. Safran, S. A., *Adv Phys.* **48,** 395 (1999).
22. Lekkerkerker, H. N. W., *Physica A* **159,** 319 (1989).
23. Safran, S. A., "Statistical Thermodynamics of Surfaces, Interfaces, and Membranes." Addison-Wesley, New York, 1994.
24. Safran, S. A., and Tlusty, T., *Ber. Bunsenges. Phys. Chem.* **100,** 252 (1996).
25. Teubner, M., and Strey, R., *J. Chem. Phys.* **87,** 3195 (1987).
26. Kahlweit, M., and Strey, R., *Angew. Chem. Int. Ed. Engl.* **24,** 654 (1985).
27. Kahlweit, M., Strey, R., Firman, P., Haase, D., Jen, J., and Schomäcker, R., *Langmuir* **4,** 499 (1988).
28. Schubert, K.-V., and Strey, R., *J. Chem. Phys.* **95,** 8532 (1991).
29. Schubert, K.-V., Strey, R., Kline, S. R., and Kaler, E. W., *J. Chem. Phys.* **101,** 5343 (1994).
30. Binks, B. P., Fletcher, P. D. I., and Taylor, D. J. F., *Langmuir* **13,** 7030 (1997).
31. Oh, K.-H., Baran, J. J., Wade, W. H., and Weerasooriya, V., *J. Dispersion Sci. Technol.* **16,** 165 (1995).
32. Pes, M. A., Aramaki, K., Nakamura, N., and Kunieda, H., *J. Colloid Interface Sci.* **178,** 666 (1996).
33. Silas, J. A., and Kaler, E. W., *Submitted* (2001).
34. Pieruschka, P., and Safran, S., *J. Phys.: Condense Matter* **6,** A357 (1994).
35. Sottmann, T., Strey, R., and Chen, S. H., *J. Chem. Phys.* **106,** 6483 (1997).